The International Journal of Robotics Research

http://ijr.sagepub.com/

New Performance Indices and Workspace Analysis of Reconfigurable Hyper-Redundant Robotic Arms

Mircea Badescu and Constantinos Mavroidis

The International Journal of Robotics Research 2004 23: 643
DOI: 10.1177/0278364904044406

The online version of this article can be found at:
http://ijr.sagepub.com/content/23/6/643

Published by:

http://www.sagepublications.com

On behalf of:

Multimedia Archives

Additional services and information for *The International Journal of Robotics Research* can be found at:

Email Alerts: http://ijr.sagepub.com/cgi/alerts

Subscriptions: http://ijr.sagepub.com/subscriptions

Reprints: http://www.sagepub.com/journalsReprints.nav

Permissions: http://www.sagepub.com/journalsPermissions.nav

Citations: http://ijr.sagepub.com/content/23/6/643.refs.html

>> Version of Record - Jun 1, 2004

What is This?

Downloaded from ijr.sagepub.com at UNIV OF WISCONSIN MILWAUKEE on October 12, 2014

Mircea Badescu

Jet Propulsion Laboratory
California Institute of Technology
Pasadena, CA 91109-8099, USA

Constantinos Mavroidis

Robotics and Mechatronics Laboratory
Department of Mechanical, Industrial
and Manufacturing Engineering
Northeastern University
Boston, MA 02115, USA
mavro@coe.neu.edu

New Performance Indices and Workspace Analysis of Reconfigurable Hyper-Redundant Robotic Arms

Abstract

In this paper, we introduce new performance indices to characterize the workspace of reconfigurable hyper-redundant robotic arms. These indices are then used to analyze the workspace of a type of hyper-redundant robotic arm using as modules lower mobility parallel platforms. The modules of the reconfigurable robotic arm are the three-legged translational universal–prismatic–universal (UPU) and orientational universal–prismatic–spherical (UPS) parallel platforms. Each arm is composed of a large number of these modules having a very large number of degrees of freedom. Results of the workspace analysis are presented in tabular and graphical forms and the corresponding best designs are identified. All possible arm assembly configurations with two, three, and four parallel platform modules and one configuration with five parallel platform modules have been taken into consideration, analyzed, and compared.

KEY WORDS—reconfigurable robots, parallel platforms, workspace analysis

1. Introduction

In recent years, modular robots were increasingly proposed as means to develop reconfigurable and self-repairable robotic systems (McKee and Schenker 1999). To perform impromptu custom tasks, increase the payload-to-weight ratio, and, in cases of emergency, self-repair, future inter-planetary robots and manipulation systems need to incorporate modularity and self-reconfiguration capabilities. Modular robots utilize many autonomous units, or modules, that can be reconfigured into a vast number of designs. Ideally, the modules will be homogeneous, small, and self-contained. The robot can change from one configuration to another by manual reassembly, or by itself. Self-reconfiguring robots adapt to a new environment or function by changing shape. Modules must interact with one another and cooperate in order to realize self-reconfiguration. Also, modular robots can repair themselves by removing and replacing failed modules. Because one self-reconfigurable modular robot can provide the functionality of many traditional mechanisms, they will be especially suited for space and planetary exploration, where payload mass must be minimum. Because they promise self-reparability and virtually limitless functionality, future self-reconfigurable modular robots are expected to be cheaper and more useful than current robot mechanisms in space missions.

Much research has been performed in the area of modular reconfigurable and self-repairable robotic systems. Here, we present a summary of some important results in this area. Modular manipulator arms have been developed such as the Modular Motion Systems' "Puma" (Schonlau 1999), and Carnegie Mellon University's Reconfigurable Modular Manipulator System (RMMS; Paredis, Brown, and Khosla 1996). Perhaps the best-tested physical prototype of a mobile modular reconfigurable robot is Rensselaer Polytechnic Institute's "Tetrobot" (Hamlin and Sanderson 1997). The Tetrobot has a tetrahedral architecture composed of links, nodes, and linear actuators. By actuating the link lengths, the Tetrobot can self-reconfigure for several different functions, including a robotic arm, a six-legged walker, and an octahedral platform. Tetrobot's large size (of the order of 1.5 m) and mass and module complexity prevent it from being considered for field missions. On a smaller scale, Xerox has introduced Polypod and its successor, Polybot (Casal and Yim 1999; Yim, Duff, and Roufas 2000). USC's CONRO robot has the same locomotive versatility as the Xerox robots (Will, Castano, and

The International Journal of Robotics Research
Vol. 23, No. 6, June 2004, pp. 643-659,
DOI: 10.1177/0278364904044406
©2004 Sage Publications

Downloaded from ijr.sagepub.com at UNIV OF WISCONSIN MILWAUKEE on October 12, 2014

Shen 1999; Castano and Will 2000; Castano, Shen, and Will 2000). Japan's Communications Research Laboratory introduced a modular robot designed only for space operations. The robot will be a part of their Orbital Maintenance System, which will inspect, repair, and re-orbit satellites (Kimura et al. 1999). Carnegie Mellon's "I-Cubes" consists of two different modules: passive cubes and active three-degrees-of-freedom (3-DoF) joints (Unsal, Kiliccote, and Khosla 1999; Unsal and Khosla 2000). Joints can attach and detach from any cube side, and can lift and move one cube at a time. Therefore, joints serve as connectors and manipulators. A more radical module design is the "Crystalline Robot" from Dartmouth's Robotics Laboratory (Rus and Vona 1999, 2000). The Crystal can contract and expand four of its six faces and move in relation to other Crystals by attaching and detaching from its neighbors. A self-reconfigurable robot, M-TRAN, with internal degrees of freedom and magnetic active and passive connectors has been proposed in Murata et al. (2002). Useful metrics for motion planning and self-reconfiguration of modular robots using a simulated annealing method were defined in Pamecha, Ebert-Uphoff, and Chirikjian (1997). A method for self-assembly and self-reconfiguration for a distributed mechanical system with identical components was presented in Tomita et al. (1999). A method to solve direct and inverse kinematics problems for open-loop redundant manipulators was proposed in Kelmar and Khosla (1990). Most of the existing experimental systems for reconfigurable robots are characterized by low payload-to-weight ratio. In an effort to increase the payload-to-weight ratio, modular reconfigurable robots have been proposed where the modules are frame-like structures.

In this project we investigate the use of three-legged parallel platforms as joint modules of reconfigurable robots. Parallel platforms are currently being used in many applications as multi-DoF systems with high rigidity, high payload-to-weight ratio, high precision and low inertia (Tsai 1999; Merlet 2000). These properties are also desired characteristics for the joint modules of reconfigurable robots. Six-legged, 6-DoF parallel platforms have been used as joint modules of reconfigurable robots in Hamlin and Sanderson (1997) and Lee and Sanderson (1999). However, the high number of DoF and of actively controlled joints per module increases complexity and cost. In addition, a purely 3-DoF translational or spherical motion would require activation of all six-module legs, which means an increase in energy consumption. Several other types of reconfigurable robots with parallel platform-like modules with less than six DoF per module have also been proposed (Miura, Furuya, and Suzuky 1985; Hughes, Sincarsin, and Carroll 1992; Chirikjian and Burdick 1994; Hafez, Lichter, and Dubowsky 2002). In this case the modules have coupled translational and spherical motion. Lately, special types of 3-DoF, three-legged parallel platforms with pure translational or pure spherical motion have received much attention (Gosselin and Angeles 1989; Gosselin and Hamel 1994; Tsai 1996; Di Gregorio and Parenti-Castelli 1998, 1999; Tsai and Joshi 2000). These platforms could be used as modules in reconfigurable robots so that they form hybrid kinematic chains with decoupled translation and orientation (Tsai and Joshi 2001). Decoupling of translation and orientation at the module level could considerably simplify the design, planning and control of such hyper-redundant robotic manipulators.

Figure 1 shows an example of such a hybrid system. In this example a two-arm reconfigurable robotic system is formed from a sequence of 3-DoF translational and orientational parallel platform modules. The translational platform with universal (U), prismatic (P), and universal (U) joints at each leg is called here the T(3-UPU) parallel platform module where the first letter "T" indicates that this module is capable of only translational motion. The orientational platform with universal, (U), prismatic, (P), and spherical (S) joints at each leg is called here the R(3-UPS) parallel platform module where the first letter "R" indicates that this module is capable of only orientational motion. The two parallel platforms have been chosen mainly because they are composed of almost identical parts, and so the reconfigurability can be applied at one more level: the module level. In previous work we performed an optimal design and workspace analysis of each of the two parallel platforms used as modules for this reconfigurable robotic system (Badescu, Morman, and Mavroidis 2002a, 2002b). In the present paper we are presenting the workspace analysis of the hybrid kinematic chains.

The workspace of a manipulator is defined as the set of all points that the end-effector of the manipulator can reach with at least one orientation. Several generic methods have been proposed to determine and evaluate the workspace of serial link and parallel manipulators such as those presented in Basaravaj and Duffy (1993), Merlet (2001), and Ceccarelli and Angeles (2000). To characterize the reachability properties of a robot manipulator, the workspace volume has usually been used as a performance index. However, this index cannot characterize the workspace with respect to other kinematic characteristics such as orientability (i.e., the ability to reach a point with several orientations) and isotropy (i.e., the ability to generate forces and motions of the same magnitude in all directions). Therefore, several performance indices have been proposed to characterize the workspace of a robotic system. The manipulability measure was defined by Yoshikawa (1985) as a scalar value given by the square root of the determinant of the product of the Jacobian matrix with its transpose. The condition number of the Jacobian has also been used to define the kinematic characteristic of a manipulator at a point in the workspace (Salisbury and Craig 1982). As this number approaches 1, the manipulator is called isotropic. Gosselin and Angeles (1991) proposed a global condition index based on the condition number of the Jacobian matrix. A mathematical theory for globally optimizing the kinematic dexterity of robotic mechanisms based on the workspace volume was presented in Park and Brockett (1994). The calculation

Downloaded from ijr.sagepub.com at UNIV OF WISCONSIN MILWAUKEE on October 12, 2014

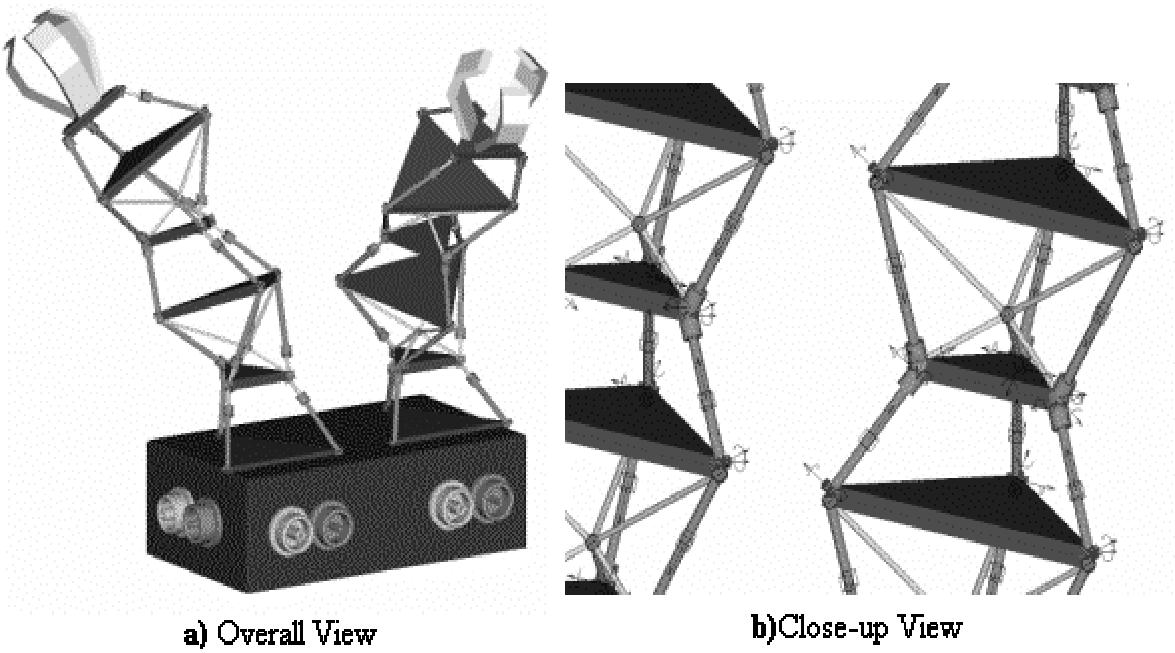

Fig. 1. Two-arm reconfigurable robot: (a) overall view; (b) close-up view.

and characterization of the global workspace of binary actuators has been performed in Zanganeh and Angeles (1997) and Ranijbaran, Angeles, and Kecskemethy (1996). A critique of these indices, as well as a review of most of the performance indices for the characterization of the workspace of robotic systems, can be found in Angeles (1995), Abdel-Malek and Yeh (2000), Sen and Mruthyunjaya (1994), and Chirikjian and Ebert-Uphoff (1998).

While most of the workspace performance indices are related to the notion of isotropy very few indices have been proposed to study the robot's orientability, i.e., the robot's ability to reach a point with many different orientations. Lee (2003) used the dexterous solid angle concept proposed in Abdel-Malek and Paul (1994) and Abdel-Malek (1995) to define the global workspace orientability volume as the integral of the dexterous solid angle over the whole workspace volume (see Section 3 for more details).

In this paper, we introduce new performance indices to characterize the workspace of reconfigurable hyper-redundant robotic arms. These indices are then used to analyze the workspace of a type of hyper-redundant robotic arm using as modules lower mobility parallel platforms. The modules of the reconfigurable robotic arm are the three-legged translational UPU and three-legged orientational UPS parallel platforms. Each arm is composed of a large number of these modules, having a very large number of degrees of freedom. Results of the workspace analysis are presented in tabular and graphical forms and the corresponding best designs are identified. All possible arm assembly configurations, with two, three, and four parallel platform modules and one configuration with five parallel platform modules, have been taken into consideration, analyzed, and compared.

2. Kinematic Description of the Arm

The hybrid hyper-redundant robot arms that are studied in this paper are composed of translational T(3-UPU) and orientational R(3-UPS) parallel platform modules. A parallel platform module is chosen as the base of the robotic arm. The next platform module is added with its base plate on top of the moving plate of the previous platform. The process is continued until the total number of parallel platform modules for that specific assembly that is being analyzed has been reached. As an example, a five-module reconfigurable hyper-redundant robotic arm with a total number of 15 DoF is presented in Figure 2. In this paper, for brevity, the T(3-UPU) translational platform is called T and the R(3-UPS) orientational/rotational platform is called R. So, in Figure 2 the TRTRT arm has as components, starting from the base, translational–orientational–translational–orientational–translational platform modules.

The T(3-UPU) parallel platform module consists of a base plate, a moving plate, and three identical limbs (see Figure 3). The plates have equilateral triangular shapes of different sizes. The limbs are connected to the plates with 2-DoF universal joints. A linear actuator controls the leg length, and forms a prismatic joint. Each universal joint is treated as two revolute

Downloaded from ijr.sagepub.com at UNIV OF WISCONSIN MILWAUKEE on October 12, 2014

Fig. 2. TRTRT robotic arm.

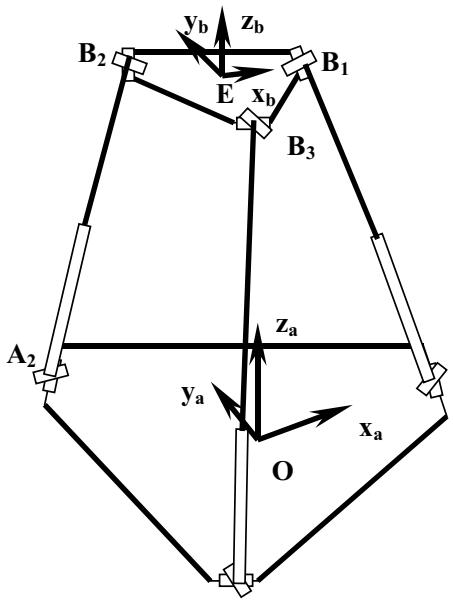

Fig. 3. The 3-UPU translational module.

joints with axes perpendicular to each other and intersecting at a point. Two parallel coordinate systems are defined: a fixed frame and a moving frame. The fixed frame, $Ox_a y_a z_a$, is defined linked to the base plate of the parallel platform with the origin at the center of the base triangle, the x-axis going through the first corner of the triangle, the z-axis perpendicular to the triangle's plane oriented upward, toward the moving plate, and the y-axis such as to obtain a right-hand Cartesian coordinate system. The moving frame, $Ex_b y_b z_b$, has the origin at the center of the moving plate.

The R(3-UPS) parallel platform module consists of a fixed tetrahedron, a moving tetrahedron, and three identical limbs (see Figure 4). The tetrahedrons have equilateral triangular bases of different sizes. The tips of the tetrahedrons are connected using a spherical joint. The limbs are connected to the moving tetrahedron base with 2-DoF universal joints and to the fixed tetrahedron base with spherical joints.

A linear actuator controls the leg length, and forms a prismatic joint. Each universal joint is treated as two revolute joints with axes perpendicular to each other and intersecting at a point. Two coordinate systems are defined: a fixed frame and a moving frame. The fixed frame, $Ox_a y_a z_a$, has the origin at the center of the triangular base plate. Its x-axis is oriented toward the fist corner of the triangle, the z-axis is perpendicular to the triangle's plane toward the rotation center (the center of the central spherical joint), and the y-axis is chosen to obtain a right-hand Cartesian coordinate system. The moving frame, $Ex_b y_b z_b$, has the origin at the center of the moving triangular plate. The x-axis is oriented toward the first corner of the triangle, the z-axis is perpendicular to the triangle's plane, away from the rotation center, and the y-axis is chosen to obtain a right-hand Cartesian coordinate system. In (0, 0, 0) orientation the two coordinate frames are parallel with each other.

The kinematic analysis of the T(3-UPU) parallel platform was performed by Tsai (1996, 1999), and used by us for optimal design (Badescu, Morman, and Mavroidis 2002a). The kinematic analysis of the R(3-UPS) parallel platform was performed by Tsai (1996) and used by us in optimal design of the module (Badescu, Morman, and Mavroidis 2002b). In these studies of the workspace of parallel platform modules, we considered constraints of the linear actuators and universal and spherical joints. Also, interference between various parts of the platform was verified. In the present work, we are using the direct and inverse kinematics of the T(3-UPU) and R(3-UPS) platforms and the workspace analysis as they have been described in Badescu, Morman, and Mavroidis (2002a, 2002b).

The kinematic assembly of the hyper-redundant robotic arm starts by selecting a base module of the type specified by the arm pattern (translational or orientational). The base coordinate frame of the first module is taken as the robotic arm's base coordinate system. A random position/orientation of the moving frame for the first module is selected. For that random configuration, the inverse kinematics problem of the parallel platform module is solved and the platform's workspace analysis is performed. If the random configuration is outside the platform's workspace, then a new random configuration is selected. The next step is to add the next module on top of the

Downloaded from ijr.sagepub.com at UNIV OF WISCONSIN MILWAUKEE on October 12, 2014

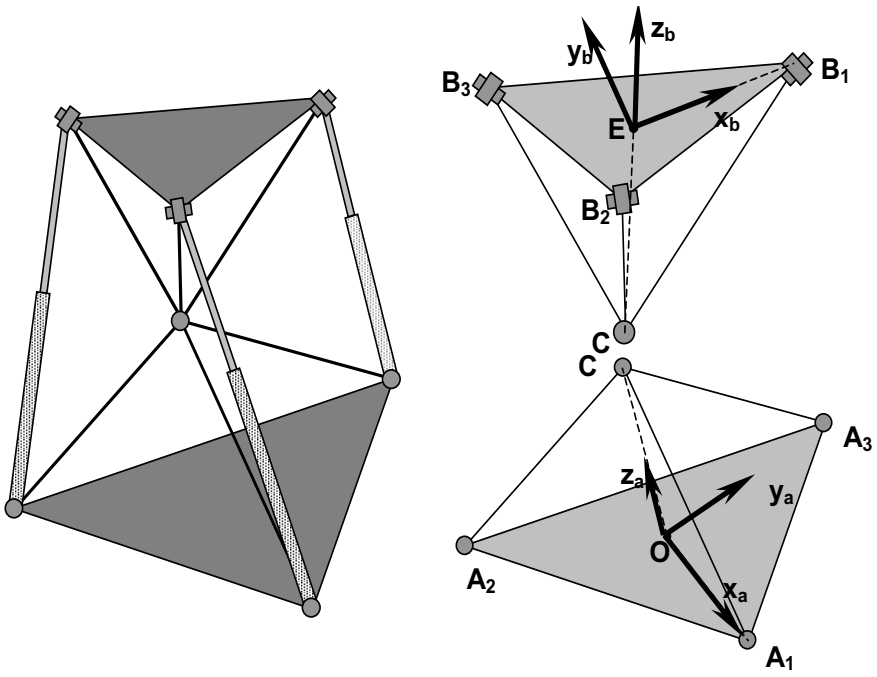

Fig. 4. The 3-UPS orientational module.

previous module selecting a random position/orientation of its moving frame with respect to its base frame. In a similar way as with the first module, the new module inverse kinematics and workspace analysis are performed. Then, the coordinates of the corners of the base and moving plates of the added module are determined with respect to the robotic arm's base coordinate system using a simple coordinate transformation. The interference between the added module and the previous module/modules is verified (see Section 4 for more details). If an interference is detected another attempt to add a new module in a random position/orientation is made. The step of adding a new module is repeated until the full arm assembly is completed. Each added module is checked for intersection with all previous modules. For the full arm assembly, the position and orientation of the end-effector, which is the moving plate of the last module, is determined with respect to the robotic arm's base coordinate system.

3. Workspace Performance Indices

In this section we define the performance indices used in this work to perform the workspace characterization of the modular robotic arms. The dexterous solid angle concept is the basis for the definitions of performance indices for hyper-redundant robot manipulators used in this paper.

Figure 5 shows a point denoted by the symbol "x", in the workspace of a redundant manipulator that can be reached by two or more configurations (configurations 1 and 2). A service sphere is defined around the point. A redundant manipulator would reach that point in more than one configuration and intersect the service sphere at more than one point. The points where the end-effector axis intersects the service sphere are called service points. The set of all service points on the sphere form a service region. The dexterous solid angle, $D(x)$, is defined as the ratio of the total area of the service regions, $A_R(x)$, to the area of the service sphere, A_S, at the point x of the end-effector (Abdel-Malek and Paul 1994)

$$D(x) = \frac{A_R(x)}{A_S} = \frac{A_R(x)}{4\pi r^2} \tag{1}$$

where r is the radius of the service sphere.

Because the dexterous solid angle of parallel platforms is not defined by a continuous function, numerical methods are used to calculate its integral. The procedure starts by defining an enclosure box that includes all the workspace points. The enclosure box can be initially a cube with the length of the edge double the maximum length of the robotic arm. The program can be run once with a lower resolution, determining the actual limits of the workspace and then using those limits to define the enclosure box. The enclosure box is divided into $N_x \times N_y \times N_z$ equal volume boxes (see Figure 6). N_x is the number of boxes on the side of the enclosure box parallel with the x coordinate axis, N_y is the number of boxes on the side of the enclosure box parallel with the y-axis, and N_z is the number of boxes on the side of the enclosure box parallel with the z-axis.

Downloaded from ijr.sagepub.com at UNIV OF WISCONSIN MILWAUKEE on October 12, 2014

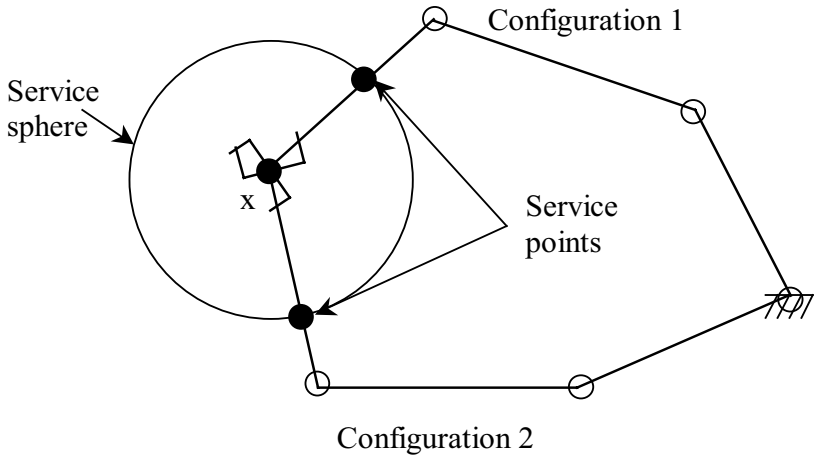

Fig. 5. The dexterous solid angle.

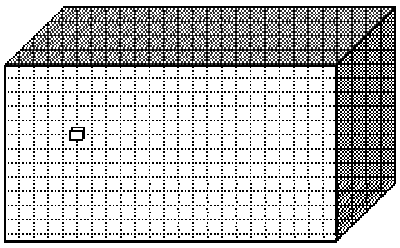

Fig. 6. Enclosure box.

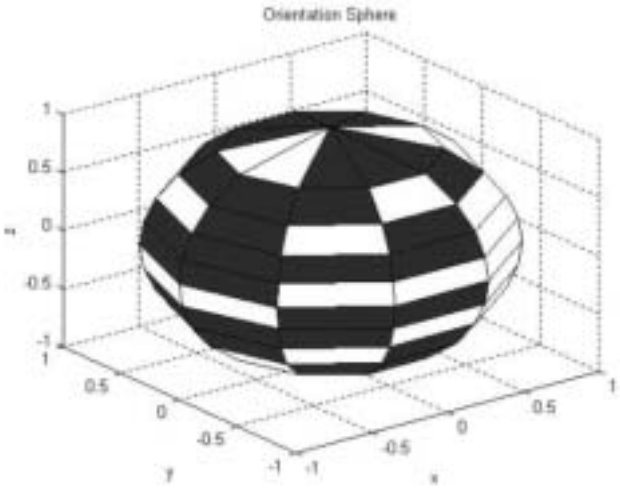

Fig. 7. Orientation sphere.

For each small box, an orientation sphere of unit radius is defined and divided into $P \times Q$ equal area patches, in latitude and longitude (see Figure 7). P is the number of strips in longitude and Q is the number of strips in latitude. The values of P and Q are determined by the orientation resolution that one wishes to achieve for a patch that is positioned at the "equator" of the orientation sphere. For example, for a $4^\circ \times 4^\circ$ resolution one needs $P = 90$ strips in longitude and $Q = 45$ strips in latitude. The strips are equally spaced in longitude. The angles at which the sphere is divided into strips in latitude are defined by eq. (2), which is derived from the condition that the area of each patch is $1/(P*Q)$ of the total area of the sphere:

$$\varphi_i = \arccos(1 - \frac{2i}{Q}), \quad \text{where } i = 0 \ldots Q. \qquad (2)$$

Figure 7 shows an example of a low-resolution orientation sphere with the reached patches filled.

The following performance indices are defined for the characterization of the workspace of the hyper-redundant robot manipulators and for each one of them the numerical calculation method is outlined as follows.

1. The workspace volume (V_W) determines the volume of the space that can be reached by the end-effector in at least one orientation. As all the linear dimensions are normalized with respect to the maximum length of the legs, which is taken as one unit (u), the workspace volume is determined in cubic units (u^3). The index is calculated as the sum of the volumes of the boxes with at least one point reached by the end-effector or as the ratio of the reached boxes over the total number of boxes multiplied with the volume of the enclosure box:

Downloaded from ijr.sagepub.com at UNIV OF WISCONSIN MILWAUKEE on October 12, 2014

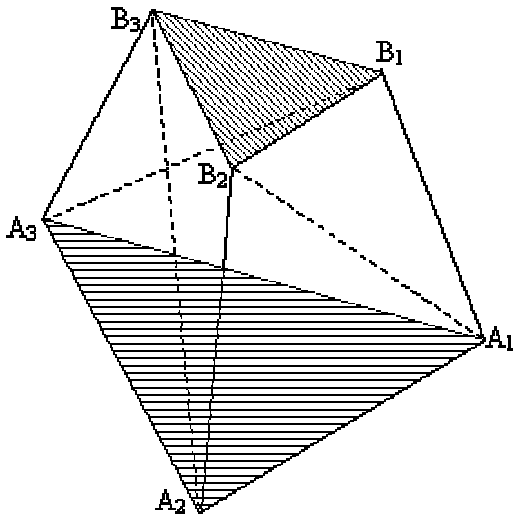

Fig. 8. Component triangles.

$$V_W = \int_{v \in W} dv \tag{3a}$$

$$V_W = \frac{K}{N_x \times N_y \times N_z} V_{initial}. \tag{3b}$$

2. The dexterous workspace volume (V_{WD}) shows how much of the reachable/workspace volume is also dexterous. It is defined as the integration of the dexterous solid angle over the whole workspace volume. The index is calculated as the ratio of the number of reached patches to the total number of patches in reached boxes, multiplied by the workspace volume:

$$V_{WD} = \int_{v \in W} D(x) dv \tag{4a}$$

$$V_{WD} = \frac{\sum_{i=1}^{K} D_i}{K \times P \times Q} \times V_w. \tag{4b}$$

3. The dexterity index (I_D) shows what percentage of the reachable volume is also dexterous. The index is calculated as the ratio of the number of reached patches over the total number of patches in reached boxes multiplied by 100:

$$I_D = \frac{\sum_{i=1}^{K} D_i}{K \times P \times Q} \times 100(\%). \tag{5}$$

4. The workspace volume with a certain dexterity ($\boldsymbol{V}_i$) is defined as the volume of the space where the dexterous solid angle has at least a certain value. The index is calculated as the ratio of the number of boxes with at least K_i reached patches over the total number of boxes in the enclosure box, multiplied by the volume of the enclosure box. It can also be defined in index form as a percentage of the number of boxes with certain dexterity out of the total number of boxes reached by the end-effector. In this paper, three values for the number of patches K_i (i= 100, 500, and 1000) are considered:

$$V_{100} = \frac{K_{100}}{N_x \times N_y \times N_z} \times V_{initial} \tag{6a}$$

$$V_{500} = \frac{K_{500}}{N_x \times N_y \times N_z} \times V_{initial} \tag{6b}$$

$$V_{1000} = \frac{K_{1000}}{N_x \times N_y \times N_z} \times V_{initial}. \tag{6c}$$

Here, K is the total number of boxes reached by the end-effector, D_i is the total number of patches in the box i reached by the end-effector, and K_{100}, K_{500}, and K_{1000} are the numbers of boxes in which the end-effector reached at least 100, 500, and 1000 patches, respectively.

4. Checking Module Interference

As described in Section 2, when a new module is added on the kinematic chain the interference of components is checked within the module and with components of the previous modules. Component interference within the module is performed using our methods presented in Badescu, Morman, and Mavroidis (2002a, 2002b). The method to determine component interference between different modules is described in this section. If any type of interference is detected, then workspace points corresponding to that configuration were excluded from the workspace.

For the interference check, both orientational and translational modules are approximated by octahedrons with triangular faces. Figure 8 shows a generic three-legged platform. The eight triangles are taken as $A_1A_2A_3$, $A_1B_2A_2$, $A_1B_1B_2$, $A_3B_1A_1$, $A_3B_3B_1$, $A_2B_3A_3$, $A_2B_2B_3$, and $B_1B_2B_3$. For triangle–triangle intersection we used the algorithm and software functions developed by Moller (1997). For platform module intersection, each triangle of the second module is checked against the intersection with every triangle of the first module. The modules intersect and the algorithm stops when a first triangle–triangle intersection is detected. If no triangle–triangle intersection is detected in any of the 64 possible situations, then the modules do not interfere with each other.

An example of such interference is shown in Figure 9. The bottom platform ($A_{11}A_{12}A_{13}B_{11}B_{12}B_{13}$) is orientational and the

Downloaded from ijr.sagepub.com at UNIV OF WISCONSIN MILWAUKEE on October 12, 2014

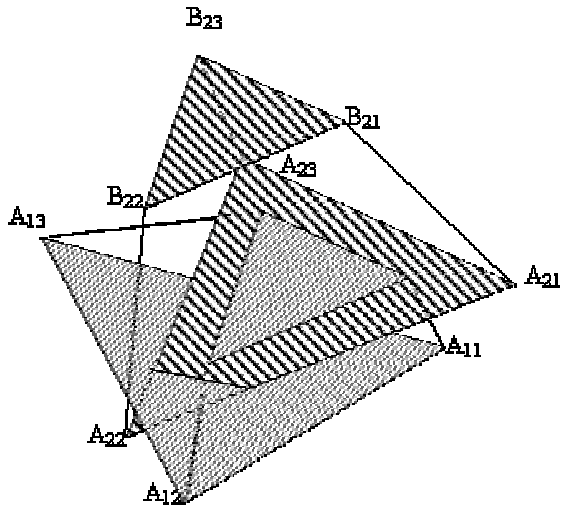

Fig. 9. Platform–platform interference.

Fig. 10. The TT assembly.

top platform ($A_{21}A_{22}A_{23}B_{21}B_{22}B_{23}$) is translational (the B_{11}, B_{12}, and B_{13} corners are not represented in the figure as they are in the same plane as A_{21}, A_{22}, and A_{23} corners). The base and moving plates corresponding to the same platform are filled with the same pattern. Also, the base plate of the top platform and the moving plate of the bottom platform are in the same plane and their centers coincide. The moving plate of the bottom platform is tilted at some angle relative to its base platform. Consequently, the base plate of the top platform is tilted to the same angle, relative to the base plate of the bottom platform. For a larger value of this angle, it is possible that the two base plates intersect each other in a posture that is not possible from a practical point of view. This is why these configurations need to be excluded from those that define the workspace of the modular robotic arm.

5. Workspace Computation Algorithm

The algorithm to calculate the workspace and its performance indices starts with the definition of the enclosure box limits and the grid resolution for the position and orientation. A binary array is defined to store information about the reached boxes. Another binary array is defined to store information about the orientation patches that are reached by the end-effector. All the elements of the two arrays are initialized with 0 (FALSE) values.

For a certain assembly, the program builds the robotic arm and determines the position and orientation of the end-effector as explained in Section 2. The corresponding workspace box that includes the end-effector's position is marked ON. From the orientation of the end-effector (i.e., the orientation of the z-axis of the moving frame of the last module) the latitude and longitude are determined and the corresponding orientation patch is marked ON.

The algorithm of determining a new successful robotic arm configuration repeats for 200,000 times. Then all the boxes and patches marked ON are counted.

The cycle of determining a set of 200,000 random successful robotic arm positions starts over. It stops when the ratio of the number of new added patches during a cycle over the total number of reached patches drops below a predefined relative value (e.g., 0.0002%). From running the program for different arm configurations, we observed that the search is actually exhaustive as the number of newly found patches drops suddenly to zero after a large enough number of cycles.

The program determines the following.

- The total number of boxes reached by the end-effector. This is used to calculate the workspace volume, V_W, using eq. (3b).
- The total number of reached patches. This is used to calculate the dexterous workspace volume, V_{WD}, and the dexterity index, I_D, using eqs. (4) and (5), respectively.
- The total number of patches reached in each box, which is used to plot the arm's workspace. The color with which the points in the workspace are plotted reflects the number of orientation patches reached in each box or the dexterous solid angle (see Section 6).
- The total number of boxes where the number of orientation patches reached is above a specific value. In this paper the boxes with 100, 500, and 1000 patches are considered. These numbers are used to calculate the workspace volumes with a certain dexterity (V_{100}, V_{500}, V_{1000}) using eqs. (6a), (6b), and (6c).
- The limits of the workspace in x, y, z Cartesian coordinates.
- The limits of the latitude and longitude that can be reached.

Downloaded from ijr.sagepub.com at UNIV OF WISCONSIN MILWAUKEE on October 12, 2014

- The most dexterous box. The data are used to plot the service region at that point. Some examples are shown in the next section.

6. Results

All possible assemblies with two, three and four platform modules and one configuration with five platform modules have been analyzed and compared. Table 1 shows the limits of the search volume and the search resolution. The limitation in resolution was mainly due to the memory limit of the computer used. The orientation resolution was maintained the same for all configurations that have at least one orientation module. In Table 1 the arm assemblies are grouped by the number of platform modules. For the two-platform arm assemblies there are four possibilities: RR, RT, TR, and TT. For the three-platform arm assemblies there are nine possibilities, and for the four-platform arm assemblies there are 16 possible cases.

Tables 2 and 3 show the values of the performance indices for each analyzed assembly. The workspace volume is presented both as a percentage of the search volume and as a physical volume. For the physical volume, the lengths used have been normalized by dividing them by the maximum leg length of the platform modules. These results can be used in two different ways for design purposes. We can select the actuators and joints, calculate the maximum length of the assembled leg, and then determine the actual workspace volume for a specific arm configuration. Also, given a specific workspace volume and dexterity, we can select a robotic arm assembly, determine the maximum leg length to enclose the required workspace volume, and select the proper actuators and joints. As an example, after selecting the type of the arm assembly the workspace volume (V_W) is given in cubic units. These units are the maximum leg length of the parallel platform modules. By equalizing the workspace volume of the arm assembly (V_W) with the task's workspace volume, the exact value of the units is determined and implicitly the maximum length of the platform legs. Having the maximum length of the leg, the linear actuators and the joints can be selected.

The dexterous workspace volume is presented as a percentage of the workspace volume and as a physical volume. The workspace volume with certain dexterity is also presented as a percentage of the workspace volume and as a physical volume. This index can be used in situations when certain dexterity (percentage of the orientation sphere) is necessary in all points of the workspace. Table 4 presents the workspace limits and the orientation limits for each configuration. It can be seen that the orientation limits are smaller than the bare multiplication of the individual orientation limits with the total number of orientational platform modules in a specific configuration. This orientation reduction/limitation is due to platform–platform interference. From Table 2 it can be seen that using the workspace volume as the evaluation criterion, for the two-platform modules the TT assembly is the best. The modular robotic arm is shown in Figure 10 and the workspace in Figure 11. Because of the lack of orientation platforms, the dexterous workspace volume is not discussed for this platform. Taking the dexterous workspace volume as the evaluation criterion, the TR configuration is the best. Pictures of all analyzed assemblies and plots of their workspace and service region of the most dexterous point for each assembly are included in Badescu (2003).

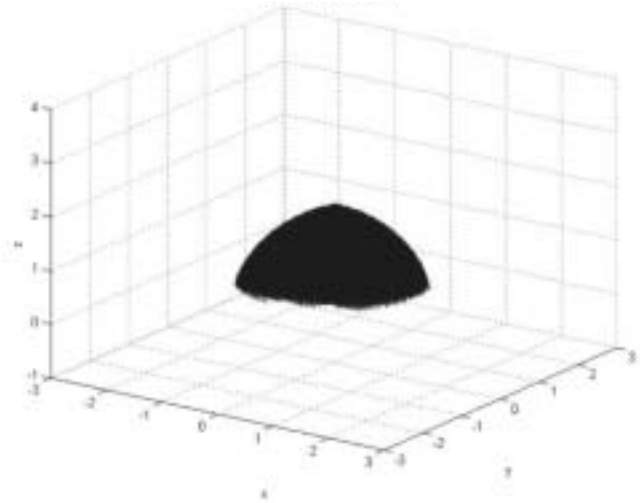

Fig. 11. The TT workspace.

Fig. 12. The TTR assembly.

For the three-platform module assembly, the largest workspace volume is obtained by the RTT configuration and the largest dexterous workspace volume is obtained by the TTR configuration. Figure 12 shows the TTR arm assembly. Figure 13 shows the workspace plot of this platform. To obtain a representation of the workspace, the centers of reached boxes were plotted using MATLAB™. The same coordinate

Downloaded from ijr.sagepub.com at UNIV OF WISCONSIN MILWAUKEE on October 12, 2014

Table 1. Search Volume and Resolution

	Search Volume			Resolution				
Assembly	$x(u)$	$y(u)$	$z(u)$	x	y	z	Longitude (deg)	Latitude (deg)
Two platform modules								
RR	2.00	2.00	1.00	60	60	30	90	90
RT	2.00	2.00	2.00	40	40	40	90	90
TR	2.00	2.00	2.00	40	40	40	90	90
TT	4.00	4.00	2.00	400	400	200	0	0
Three platform modules								
RRR	2.50	2.50	1.50	50	50	30	90	90
RRT	3.00	3.00	2.25	60	60	45	90	90
RTR	3.00	3.00	2.00	60	60	40	90	90
RTT	4.00	4.00	3.00	60	60	45	90	90
TRR	2.50	2.50	1.50	50	50	30	90	90
TRT	3.60	3.60	2.60	54	54	39	90	90
TTR	3.20	3.20	1.75	64	64	35	90	90
TTT	5.00	5.00	2.50	500	500	250	0	0
Four platform modules								
RRRR	3.50	3.50	2.50	35	35	25	90	90
RRRT	4.00	4.00	3.00	40	40	30	90	90
RRTR	4.00	4.00	3.00	40	40	30	90	90
RRTT	5.00	5.00	3.80	50	50	38	90	90
RTRR	4.00	4.00	3.00	40	40	30	90	90
RTRT	4.60	4.60	3.50	46	46	35	90	90
RTTR	4.60	4.60	3.30	46	46	33	90	90
RTTT	5.20	5.20	4.00	52	52	40	90	90
TRRR	3.60	3.60	2.00	54	54	30	90	90
TRRT	4.00	4.00	3.00	60	60	45	90	90
TRTR	4.00	4.00	2.60	60	60	39	90	90
TRTT	5.00	5.00	3.50	50	50	35	90	90
TTRR	4.00	4.00	2.00	60	60	30	90	90
TTRT	5.00	5.00	3.00	50	50	30	90	90
TTTR	4.40	4.40	2.40	66	66	36	90	90
TTTT	5.30	5.30	2.75	530	530	275	0	0
Five platform modules								
TRTRT	6.00	6.00	5.00	60	60	50	90	90

Downloaded from ijr.sagepub.com at UNIV OF WISCONSIN MILWAUKEE on October 12, 2014

Table 2. Performance Indices (1)

Assembly	Search Volume (u^3)	Workspace Volume (V_W) (%)	Workspace Volume (V_W) (u^3)	Dexterity Index (I_D) (%)	Dexterous Workspace Volume (V_{WD}) (u^3)
Two platform modules					
RR	4.00	2.64	0.106	4.44	0.0047
RT	8.00	29.13	2.330	3.72	0.0867
TR	8.00	13.39	1.072	10.31	0.1104
TT	32.00	13.33	4.266	0.00	0.0000
Three platform modules					
RRR	9.38	11.94	1.119	6.53	0.0731
RRT	20.25	33.52	6.788	3.47	0.2358
RTR	18.00	25.99	4.678	7.74	0.3621
RTT	48.00	30.92	14.843	2.74	0.4062
TRR	9.38	30.57	2.866	10.61	0.3040
TRT	33.70	33.50	11.288	3.81	0.4295
TTR	17.92	34.30	6.147	7.94	0.4880
TTT	62.50	16.44	10.275	0.00	0.0000
Four platform modules					
RRRR	30.63	18.74	5.740	7.93	0.4553
RRRT	48.00	38.16	18.317	4.21	0.7715
RRTR	48.00	31.37	15.056	8.25	1.2422
RRTT	95.00	32.01	30.410	3.49	1.0620
RTRR	48.00	24.16	11.598	10.12	1.1733
RTRT	74.06	36.62	27.121	4.40	1.1938
RTTR	69.83	31.76	22.179	7.99	1.7717
RTTT	108.16	36.06	39.000	2.35	0.9183
TRRR	25.92	31.08	8.056	7.72	0.6216
TRRT	48.00	41.01	19.683	3.49	0.6875
TRTR	41.60	40.16	16.708	5.56	0.9288
TRTT	87.50	38.49	33.679	2.86	0.9632
TTRR	32.00	31.01	9.925	8.36	0.8294
TTRT	75.00	32.56	24.419	3.89	0.9487
TTTR	46.46	34.46	16.014	5.86	0.9378
TTTT	77.25	18.22	14.073	0.00	0.0000
Five platform modules					
TRTRT	180.00	25.74	46.330	3.43	1.5902

Downloaded from ijr.sagepub.com at UNIV OF WISCONSIN MILWAUKEE on October 12, 2014

Table 3. Performance Indices (2)

Assembly	V_{100} (%)	V_{100} (u^3)	V_{500} (%)	V_{500} (u^3)	V_{1000} (%)	V_{1000} (u^3)
Two platform modules						
RR	76.05	0.0804	30.15	0.0319	0.21	0.0002
RT	64.53	1.5036	25.45	0.5931	0.56	0.0131
TR	84.03	0.9004	63.11	0.6763	39.80	0.4265
TT	0.00	0.0000	0.00	0.0000	0.00	0.0000
Three platform modules						
RRR	65.50	0.7331	40.46	0.4529	22.62	0.2531
RRT	54.24	3.6823	22.98	1.5598	5.09	0.3458
RTR	67.47	3.1559	44.15	2.0650	27.12	1.2688
RTT	52.55	7.8003	16.88	2.5055	0.00	0.0000
TRR	71.41	2.0468	53.13	1.5226	39.07	1.1199
TRT	56.86	6.4181	28.79	3.2498	0.02	0.0018
TTR	71.32	4.3843	49.19	3.0240	32.33	1.9874
TTT	0.00	0.0000	0.00	0.0000	0.00	0.0000
Four platform modules						
RRRR	62.33	3.5780	41.95	2.4080	28.82	1.6540
RRRT	57.02	10.4440	28.57	5.2330	9.48	1.7360
RRTR	61.72	9.2930	41.80	6.2940	28.95	4.3580
RRTT	53.14	16.1590	24.50	7.4510	4.56	1.3860
RTRR	65.93	7.6460	47.51	5.5100	34.83	4.0400
RTRT	54.23	14.7070	29.71	8.0580	12.11	3.2850
RTTR	61.47	13.6330	41.17	9.1310	28.26	6.2670
RTTT	48.08	18.7510	12.79	4.9900	0.00	0.0000
TRRR	56.87	4.5810	37.38	3.0113	26.05	2.0987
TRRT	46.82	9.2157	22.68	4.4640	8.63	1.6996
TRTR	52.13	8.7093	29.74	4.9698	18.35	3.0661
TRTT	48.79	16.4330	20.10	6.7690	0.00	0.0000
TTRR	61.18	6.0717	41.18	4.0874	29.11	2.8892
TTRT	54.40	13.2840	30.06	7.3410	1.11	0.2720
TTTR	58.57	9.3790	36.10	5.7816	21.71	3.4770
TTTT	0.00	0.0000	0.00	0.0000	0.00	0.0000
Five platform modules						
TRTRT	44.67	20.6960	22.38	10.3680	9.11	4.2210

Downloaded from ijr.sagepub.com at UNIV OF WISCONSIN MILWAUKEE on October 12, 2014

Table 4. Workspace Limits

	Workspace Limits						Best Orientation			
	$x(u)$		$y(u)$		$z(u)$		Latitude (deg)		Longitude (deg)	
Assembly	min	max	min	max	min	max	min	max	min	max
Two platform modules										
RR	–0.54	0.42	–0.50	0.50	0.55	0.96	0	113.41	–180	180
RT	–0.99	0.94	–0.98	0.98	–0.01	1.44	0	53.85	–180	180
TR	–0.81	0.90	–0.87	0.87	0.63	1.44	0	62.51	–180	180
TT	–1.36	1.56	–1.45	1.46	0.47	1.90	0	0.00	0	0
Three platform modules										
RRR	–1.02	0.89	–0.98	0.97	0.35	1.44	0	153.21	–180	180
RRT	–1.49	1.34	–1.41	1.41	–0.18	1.92	0	105.14	–180	180
RTR	–1.38	1.24	–1.35	1.34	0.19	1.92	0	114.41	–180	180
RTT	–1.83	1.74	–1.79	1.78	–0.28	2.37	0	53.85	–180	180
TRR	–1.21	1.18	–1.22	1.21	0.82	1.92	0	113.39	–180	180
TRT	–1.62	1.66	–1.68	1.65	0.31	2.38	0	53.85	–180	180
TTR	–1.46	1.63	–1.55	1.56	0.90	2.38	0	62.51	–180	180
TTT	–1.98	2.25	–2.15	2.12	0.73	2.81	0	0.00	0	0
Four platform modules										
RRRR	–1.50	1.37	–1.45	1.45	–0.01	1.92	0	178.06	–180	180
RRRT	–1.93	1.78	–1.88	1.89	–0.39	2.40	0	147.59	–180	180
RRTR	–1.96	1.79	–1.89	1.88	–0.33	2.40	0	158.63	–180	180
RRTT	–2.36	2.15	–2.24	2.26	–0.80	2.85	0	105.90	–180	180
RTRR	–1.84	1.66	–1.80	1.79	0.12	2.40	0	150.87	–180	180
RTRT	–2.26	2.04	–2.14	2.16	–0.36	2.84	0	105.98	–180	180
RTTR	–2.17	2.05	–2.13	2.12	–0.03	2.85	0	113.41	–180	180
RTTT	–2.60	2.50	–2.59	2.55	–0.44	3.25	0	53.85	–180	180
TRRR	–1.69	1.65	–1.66	1.67	0.68	2.40	0	160.96	–180	180
TRRT	–2.05	2.01	–2.06	2.03	0.21	2.85	0	105.90	–180	180
TRTR	–1.98	1.91	–1.97	1.98	0.57	2.86	0	113.33	–180	180
TRTT	–2.38	2.39	–2.40	2.39	0.09	3.27	0	53.85	–180	180
TTRR	–1.83	1.90	–1.85	1.91	1.15	2.86	0	112.17	–180	180
TTRT	–2.18	2.32	–2.34	2.24	0.68	3.27	0	53.85	–180	180
TTTR	–2.00	2.31	–2.13	2.19	1.17	3.27	0	62.51	–180	180
TTTT	–2.54	2.85	–2.69	2.69	1.09	3.68	0	0.00	0	0
Five platform modules										
TRTRT	–2.76	2.65	–2.73	2.75	–0.03	3.71	0	105.98	–180	180

Downloaded from ijr.sagepub.com at UNIV OF WISCONSIN MILWAUKEE on October 12, 2014

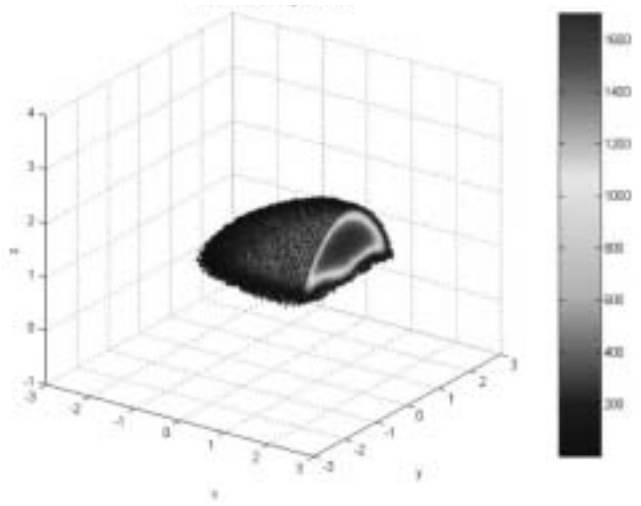

Fig. 13. The TTR workspace.

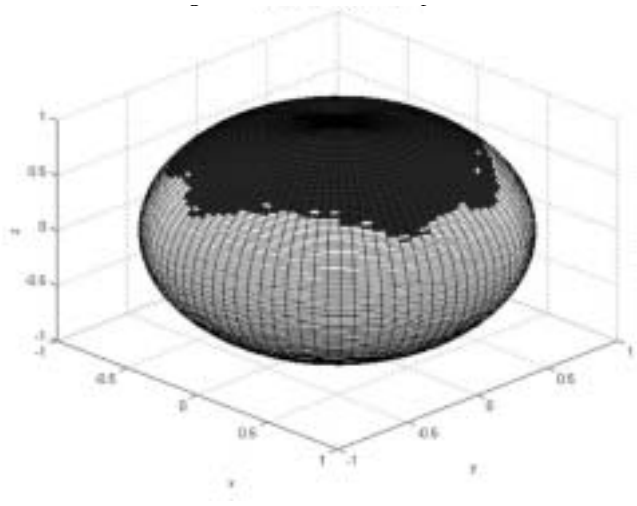

Fig. 14. The TTR service sphere.

system limits were used for all configurations to provide a relative view of the size of the workspace. The intensity of the colors of the points correspond to the dexterity of the robotic arm at that specific point (the number of different patches on the orientation sphere that can be reached by the end-effector at that location). The number in the color/intensity bar represents how many patches out of 8100 can be reached by the end-effector at that specific location. In the picture, only half of the workspace is shown to present the dexterity inside the workspace volume. Figure 14 shows the service region for the most dexterous point for the TTR arm assembly. The plot comprises a sphere divided into patches of equal area, in latitude and longitude. In the plot, the patches that can be reached by the end-effector are colored blue. The unreachable patches have only the contour drawn.

For the four-platform module assemblies, the largest workspace volume is given by the RTTT assembly and the largest dexterous volume is given by the RTTR assembly. The RTTR assembly is shown in Figure 15. Its half workspace is shown in Figure 16 and the service sphere of the most dexterous point is shown in Figure 17. For the RTTR configuration, a higher value of the dexterous workspace volume is mainly due to a larger number of points with high dexterity against the fact that the workspace volume is reduced (see Tables 2 and 3). Out of all configurations that have been studied in this work, using the dexterous workspace volume as the comparison criterion, RTTR is the best configuration. It outperforms even the TRTRT five-platform module assembly (see Table 2).

Fig. 15. The RTTR assembly.

7. Conclusions

In this paper we have presented performance indices to characterize the workspace of hybrid, hyper-redundant manipulators and an analysis and comparison of robotic arms using parallel platforms as modules. We have defined and described performance indices that describe the workspace volume, the workspace volume and dexterity, and the workspace volume with certain dexterity, and we have explained how they are calculated. An analysis using these performance indices was performed for all possible two-, three-, and four-platform module assemblies and one five-platform module assembly. The values for all performance indices are presented in tabular forms and the best designs are identified. We have also made suggestions about how to use these tables for the selection of a certain assembly for a task. Using as a comparison criterion the dexterous workspace volume, it has been shown that the

Downloaded from ijr.sagepub.com at UNIV OF WISCONSIN MILWAUKEE on October 12, 2014

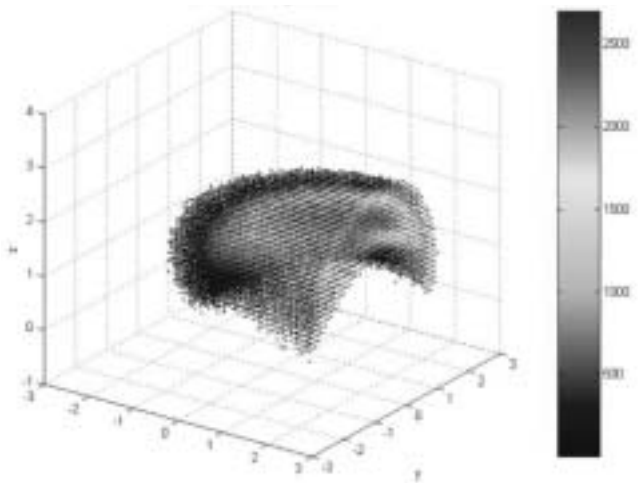

Fig. 16. The RTTR workspace.

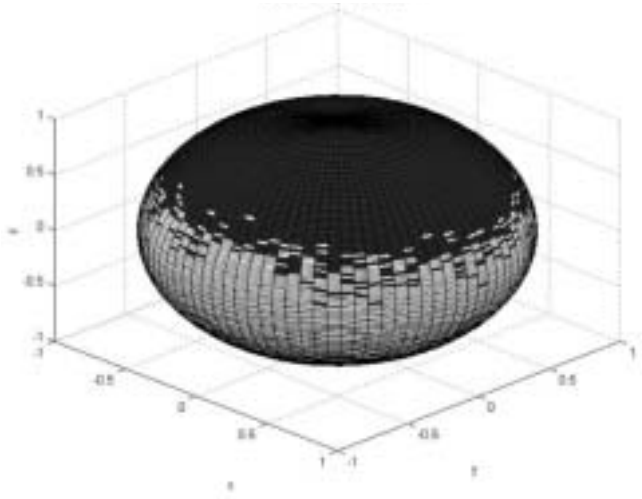

Fig. 17. The RTTR service sphere.

best assembly among the two-platform module assemblies is the TR. For the three-platform modules the best design is the TTR assembly and for the four-platform modules the best design is the RTTR assembly. The RTTR assembly even outperforms a five-platform module assembly, the TRTRT. For these designs, plots are also presented showing the workspace and the service sphere for the best orientation position.

Acknowledgments

This work was supported by a National Science Foundation CAREER Award (DMI-9984051). The authors would like to thank Eric Lee for the discussions and suggestions regarding dexterous workspace volume index.

References

Abdel-Malek, K. 1995. Dexterity of manipulator arms at an operating point. *Proceedings of the 21st ASME Advances in Design Automation*, DE Vol. 82, No. 1, pp. 781–788.

Abdel-Malek, K. and Paul, B. 1994. The dexterous solid angle for manipulators with a spherical wrist. *Proceedings of the 23rd ASME Mechanisms Conference*, Minneapolis, MN, pp. 341–350.

Abdel-Malek, K. and Yeh, H. J. 2000. Atlases of orientability for robotic manipulator arms. *IASTED International Journal of Robotics and Automation* 15(4):189–205.

Angeles, J. 1995. Kinematic isotropy in humans and machines. *Proceedings of the 9th World Congress on the Theory of Machines and Mechanisms*, Milan, Italy, August 29–September 2, Vol.1, pp. XLII–XLIX.

Badescu, M. 2003. *Reconfigurable Robots Using Parallel Platforms as Modules*, PhD Thesis, Rutgers University, May.

Badescu, M., Morman, J., and Mavroidis, C. 2002a. Workspace optimization of 3-UPU parallel platforms with joint constraints. *Proceedings of the 2002 IEEE International Conference of Robotics and Automation*, Washington, DC, May 11–15, pp. 3678–3683.

Badescu, M., Morman, J., and Mavroidis, C. 2002b. Workspace optimization of orientational 3-legged UPS parallel platforms. *Proceedings of the 2002 ASME International Design Engineering Technical Conferences and the Computers and Information in Engineering Conference (DETC/CIE)*, Montreal, Canada, September, DETC2002/MECH-34366.

Basaravaj, U., and Duffy, J. 1993. End-effector motion capabilities of serial manipulators. *International Journal of Robotics Research* 12(2):132–145.

Casal, A., and Yim, M. 1999. Self-reconfiguration planning for a class of modular robots. *Proceedings of SPIE Sensor Fusion and Decentralized Control II*, Boston, MA, September, pp. 246–257.

Castano, A., and Will, P. 2000. Mechanical design of a module for autonomous reconfigurable robots. *Proceedings of the IEEE/RSJ International Conference on Intelligent Robots and Systems (IROS2000)*, Takamatsu, Japan, November, pp. 2203–2209.

Castano, A., Shen, W.-M., and Will, P. 2000. CONRO: towards deployable robots with inter-robot metamorphic capabilities. *Autonomous Robots* 8(3):309–324.

Ceccarelli, M., and Angeles, J. 2000. A numerical evaluation of the workspace of a seven-axis, redundant manipulator. *Proceedings of the 2001 IEEE International Conference on Robotics and Automation, ICRA2000*, San Francisco, CA, April 24–28, pp. 2551–2556.

Chirikjian, G. S., and Burdick, J. W. 1994. A modal approach to hyper-redundant manipulator kinematics. *IEEE Transactions on Robotics and Automation* 10(3):343–354.

Downloaded from ijr.sagepub.com at UNIV OF WISCONSIN MILWAUKEE on October 12, 2014

Chirikjian, G. S., and Ebert-Uphoff, I. 1998. Numerical convolution on the Euclidean group with applications to workspace generation. *IEEE Transactions on Robotics and Automation* 14(1):123–136.

Di Gregorio, R., and Parenti-Castelli, V. 1998. A translational 3-DoF parallel manipulator. *Advances in Robot Kinematics: Analysis and Control*, J. Lenarcic and M. L. Husty, editors, Kluwer Academic, Dordrecht, pp. 49–58.

Di Gregorio, R., and Parenti-Castelli, V. 1999. Mobility analysis of the 3-UPU parallel mechanism assembled for a pure translational motion. *Proceedings of the 1999 IEEE/ASME International Conference on Advanced Intelligent Mechatronics, AIM'99*, Atlanta, GA, September 19–23, pp. 520–525.

Gosselin, C., and Angeles, J. 1989. The optimum kinematic design of a spherical three-degree-of-freedom parallel manipulator. *ASME Journal of Mechanisms, Transmissions, and Automation in Design* 111(2):202–207.

Gosselin, C., and Angeles, J. 1991. A global performance index for the kinematic optimization of robotic manipulators. *ASME Journal of Mechanical Design* 113(3):220–226.

Gosselin, C., and Hamel, J. 1994. The agile eye: a high-performance three-degree-of-freedom camera-orienting device. *Proceedings of the IEEE International Conference on Advanced Robotics*, Pisa, Italy, pp. 781–786.

Hafez, M., Lichter, M. D., and Dubowsky, S. 2002. Optimized binary modular reconfigurable robotic devices. *Proceedings of the IEEE International Conference on Robotics and Automation, ICRA'02*, Washington, DC, May 11–15, Vol. 1, pp. 335–340.

Hamlin, G., and Sanderson, A. 1997. TETROBOT: a modular approach to parallel robotics. *IEEE Robotics and Automation Magazine* 4(1):42–49.

Hughes, P. C., Sincarsin, W. G., and Carroll, K. A. 1992. Trussarm—a variable-geometry-truss manipulator. *Journal of Intelligent Material Systems and Structures* 2:148–161.

Kelmar, L., and Khosla, P. K. 1990. Automatic generation of forward and inverse kinematics for a reconfigurable modular manipulator system. *Journal of Robotic Systems* 7(4):599–619.

Kimura, S., Tsuchiya, S., Nishida, S., and Takegai, T. 1999. Module type space manipulator. *Proceedings of SPIE Sensor Fusion and Decentralized Control II*, Boston, MA, September, pp. 307–315.

Lee, E. 2003. *Computational Analysis and Design of Robot Manipulators*, Masters Thesis, Rutgers University, May.

Lee, W. H., and Sanderson, A. 1999. Dynamics and distributed control of Tetrobot modular robots. *Proceedings of the 1999 IEEE International Conference on Robotics and Automation*, Detroit, MI, Vol. 4, pp. 2704–2710.

McKee, G., and Schenker, P., editors. 1999. *Sensor Fusion and Decentralized Control in Robotic Systems II*, SPIE Proceedings Series, Vol. 3839.

Merlet, J.-P. 2000. *Parallel Robots*, Kluwer, Dordrecht.

Merlet, J. P. 2001. An improved design algorithm based on interval analysis for spatial parallel manipulator with specified workspace. *Proceedings of the 2001 IEEE International Conference on Robotics and Automation*, Seoul, Korea, May 21–26, pp. 1289–1294.

Miura, K., Furuya, H., and Suzuky, K. 1985. Variable geometry truss and its applications to deployable truss and space crane arm. *Acta Astronautica* 12(7/8):599–607.

Moller, T. 1997. A fast triangle–triangle intersection test. *Journal of Graphics Tools* 2(2):25–30.

Murata, S., Yoshida, E., Kamimura, A., Kurokawa, H., Tomita, K., and Kokaji, S. 2002. M-TRAN: self-reconfigurable modular robotic system. *IEEE/ASME Transactions on Mechatronics* 7(4):431–441.

Pamecha, A., Ebert-Uphoff, I., and Chirikjian, G. S. 1997. Useful metrics for modular robot motion planning. *IEEE Transactions on Robotics and Automation* 13(4):531–545.

Paredis, C. J. J., Brown, B. H., and Khosla, P. K. 1996. A rapidly deployable manipulator system. *Proceedings of the 1996 IEEE International Conference on Robotics and Automation*, Minneapolis, MN, April, pp. 1434–1439.

Park, F. C., and Brockett, R. W. 1994. Kinematic dexterity of robotic mechanisms. *International Journal of Robotics Research* 13(1):1–15.

Ranjbaran, F., Angeles, J., and Kecskemethy, A. 1996. On the kinematic conditioning of robotic manipulators. *Proceedings of the 1996 IEEE International Conference on Robotics and Automation*, Minneapolis, MN, April, pp. 3167–3172.

Rus, D., and Vona, M. 1999. Self-reconfiguration planning with compressible unit modules. *Proceedings of the 1999 IEEE International Conference on Robotics and Automation*, Detroit, MI, May, pp. 2513–2520.

Rus, D., and Vona, M. 2000. A physical implementation of the self-reconfiguring Crystalline robot. *Proceedings of the 2000 IEEE International Conference on Robotics and Automation*, San Francisco, CA, April, pp. 1726–1733.

Salisbury, J. K., and Craig, J. J. 1982. Articulated hands: force control and kinematics issues. *International Journal of Robotics Research* 1(1):4–17.

Schonlau, W. J. 1999. MMS: a modular robotic system and model based control architecture. *Proceedings of the 1999 SPIE Conference on Sensors Fusion and Decentralized Control in Robotic Systems*, Boston, MA, September, Vol. 3839, pp. 289–296.

Sen, D., and Mruthyunjaya, T. S. 1994. A discrete state perspective of manipulator workspaces. *Mechanism and Machine Theory* 29(4):591–605.

Tomita, K., Murata, S., Kurokawa, H., Yoshida, E., and Kokaji, S. 1999. Self-assembly and self-repair method for a distributed mechanical system. *IEEE Transactions on Robotics and Automation* 15(6):1035–1045.

Tsai, L.-W. 1996. Kinematics of a three-DoF platform with

Downloaded from ijr.sagepub.com at UNIV OF WISCONSIN MILWAUKEE on October 12, 2014

three extensible limbs. *Recent Advances in Robot Kinematics*, J. Lenarcic and V. Parenti-Castelli, editors, Kluwer Academic, Dordrecht, pp. 401–410.

Tsai, L.-W. 1999. *Robot Analysis—The Mechanics of Serial and Parallel Manipulators*, Wiley, New York.

Tsai, L. W., and Joshi, S. 2000. Kinematics and optimization of a spatial 3-UPU parallel manipulator. *ASME Transactions, Journal of Mechanical Design* 122(4):439–446.

Tsai, L. W., and Joshi, S. 2001. Feasibility study of hybrid kinematics machines. *Proceedings of the 2001 NSF Design, Manufacturing and Industrial Innovation Research Conference*, Tampa, FL, January 7–10.

Unsal, C., and Khosla, P. 2000. Mechatronic design of a modular self-reconfiguring robotic system. *Proceedings of the 2000 IEEE International Conference on Robotics and Automation*, San Francisco, CA, April, pp. 1742–1747.

Unsal, C., Kiliccote, H., and Khosla, P. 1999. I(CES)-Cubes: a modular self-reconfigurable bipartite robotic system. *Proceedings of 1999 SPIE Conference on Sensors Fusion and Decentralized Control in Robotic Systems*, Boston, MA, September, Vol. 3839, pp. 258–269.

Will, P., Castano, A., and Shen, W.-M. 1999. Robot modularity for self-reconfiguration. *Proceedings of SPIE Sensor Fusion and Decentralized Control II*, Boston, MA, September, pp. 236–245.

Yim, M., Duff, D. G., and Roufas, K. D. 2000. Polybot: a modular reconfigurable robot. *Proceedings of the 2000 IEEE International Conference on Robotics and Automation*, San Francisco, CA, April, pp. 514–520.

Yoshikawa, T. 1985. Manipulability of robotic mechanisms. *International Journal of Robotics Research* 4(2):3–9.

Zanganeh, K. E., and Angeles, J. 1997. Kinematic isotropy and the optimum design of parallel manipulators. *International Journal of Robotics Research* 16(2):185–197.

Downloaded from ijr.sagepub.com at UNIV OF WISCONSIN MILWAUKEE on October 12, 2014